Chapter 2
Controlling the Position and Motion of a Single Atom in an Optical Cavity

2.1 Trapping Atoms in a Cavity

CQED with single trapped atoms has a long history. The first experiments in the optical domain employed hot atomic beams, with a stepwise reduction in the number of atoms in the cavity [1], which eventually led to the observation of a normal-mode splitting with an average atom number of only one [2]. In this setting, a first measurement of the phase shift that a single atom can imprint onto a transmitted faint laser beam was demonstrated [3]. However, atom-light interaction was limited to very short times ($\sim\mu$s) in these experiments. To improve this, the techniques of laser cooling and trapping [4] were introduced to CQED. First steps along these lines were taken by releasing cold atoms from a magneto-optical trap (MOT) such that they fall through a high-finesse optical cavity [5, 6]. Interaction times were further increased with an atomic fountain with the cavity at the turning point of the atoms [7, 8]. The only way to further improve was then to employ an atom trap within the cavity.

In principle, there are two commonly used techniques for single-atom trapping: First, electrical trapping of charged atoms—usually cations [9]. Second, optical trapping of neutral atoms in far detuned laser fields [10, 11]. In cavity QED experiments, the first approach—the use of ions—has been restricted to very long cavities [12, 13] due to the technical difficulty that the dielectric mirrors of optical resonators tend to disturb the electric trapping potential. Therefore, the strong-coupling regime has not been reached with trapped ions until today, albeit there is some progress due to the development of fiber-based Fabry-Perot cavities [14] which—due to their smaller size—allow to trap an ion in a resonator of sufficiently small mode volume to fulfill the condition $g > \gamma$ [15].

In contrast, the strong-coupling regime has been achieved in many experiments with trapped neutral atoms. Remarkably, it has early been demonstrated in two independent experiments in the strong coupling regime [16, 17] that even the force of single optical photons can suffice to trap an atom when operating at a resonant

A. Reiserer, *A Controlled Phase Gate Between a Single Atom and an Optical Photon*, Springer Theses,
DOI 10.1007/978-3-319-26548-3_2

electronic transition. In all experiments that employ several atomic levels, however, a state-insensitive trap is required. In this respect, the first milestone was the achievement of a 28 ms atom storage time in a far-off-resonance dipole trap (FORT) [18], implemented in a standing-wave configuration along the cavity axis. The working principle of such a trap is explained in Sect. 2.1.1. To increase the storage time for single atoms, efficient cooling mechanisms are required. A brief summary of the various previously employed techniques is given in Sect. 2.1.2, before turning to the trap implemented in this thesis in Sect. 2.2.

2.1.1 Optical Dipole Traps

To date, all experiments that trap single atoms in a cavity in the strong-coupling regime employ optical dipole traps, which have been established as a standard technique in atomic physics, summarized in several review articles (e.g. [10, 11]) and standard textbooks (e.g. [4]). While a brief introduction to the most relevant parameters is given in the following, a more detailed discussion of the geometry and parameters of the trap implemented in this thesis will be presented in Sect. 2.2.

The origin of the confining force in an optical trap is the electromagnetic field of an intense, off-resonant laser beam. In any polarizable particle, this leads to an induced dipole moment which then interacts dispersively with the gradient of the laser field. For a two-level atom with an excited state that decays to the ground state at a rate Γ while emitting photons at a frequency ω_0, the interaction potential takes the form [10]:

$$U_{dip}\left(\vec{r}\right) = -\frac{3\pi c^2}{2\omega_0^3}\left(\frac{\Gamma}{\omega_0 - \omega} + \frac{\Gamma}{\omega_0 + \omega}\right) I\left(\vec{r}\right) \tag{2.1}$$

Here, $I\left(\vec{r}\right)$ denotes the spatially dependent laser intensity, ω the laser frequency, and c the speed of light. In a two-level system, the energy of the ground state is lowered if $\omega < \omega_0$, i.e. if the laser is detuned towards the red side of the electromagnetic spectrum. The energy of the excited state is increased by the same amount. When considering alkaline atoms rather than the idealized two-level approximation, the sum over all possible transitions has to be evaluated to calculate the overall optical potential. For ^{87}Rb, the wavelength dependence of the atomic level shifts is shown in Fig. 2.1.

The spatial structure of the ground-state potential is given by the intensity distribution of the used trapping laser. A common configuration is the use of a retro-reflected laser beam, which is also called a one-dimensional optical lattice. Along the direction of the laser beam (z), the formation of a standing-wave pattern gives rise to a modulated potential with a period of $\frac{\lambda}{2}$. Along the perpendicular axes (x, y), the potential is given by the Gaussian mode profile of the laser beam with a waist of w_0. Thus, the resulting overall potential of depth U_0 takes the form:

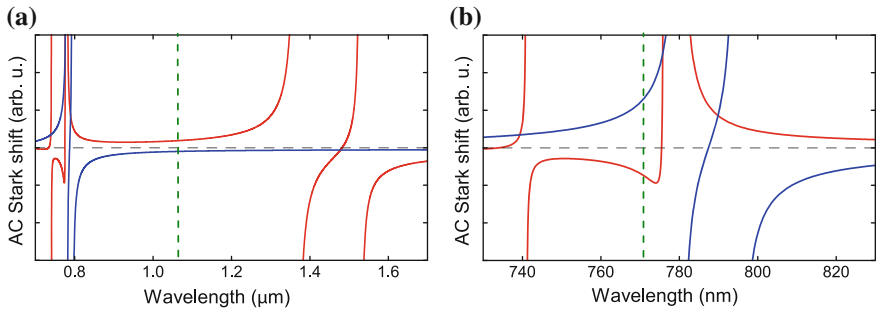

Fig. 2.1 **a** and **b** Stark shift of the atomic states $5S_{1/2}$ (*blue*) and $5P_{3/2}$ (*red*), depending on the wavelength of the trapping laser. The *dashed green lines* indicate the wavelengths of the optical lattice used in the experimental setup, described in detail in Sect. 2.2

$$U_{SW}(\vec{r}) = U_0 \cos^2\left(2\pi\frac{z}{\lambda}\right) \exp\left(-\frac{x^2+y^2}{2w_0^2}\right) \tag{2.2}$$

When several non-interfering laser beams are employed (i.e. using orthogonal polarizations), the individual potentials simply add up. The same holds when the beams have different frequencies and thus the interference pattern shifts its position on a timescale that is fast compared to the atomic motion. Close to its bottom, the trap is well approximated by a harmonic potential. In this case, the vibrational energy states are equidistant with a separation of $h\nu_{trap}$, where ν_{trap} is called the trap frequency. Along the standing-wave axis, it is given by: $\nu_{trap} = \frac{\hbar}{\lambda}\sqrt{\frac{2U_0}{m}}$.

When the trap frequency is much larger than the recoil frequency that corresponds to the momentum of a single resonant photon, the motional state of the atom does not change in most absorption and emission events. This regime is called the Lamb-Dicke regime and is very favorable for efficient laser cooling to the ground state of the potential. For Rubidium atoms, the recoil frequency is $2\pi \cdot 4\,\text{kHz}$, which means that deep potentials with trap frequencies on the order of 10–100 kHz are required. This can be achieved with high laser intensities, however at the price of increased heating and ground-state decoherence, since the rate at which the atom scatters trap light is given by:

$$R_{scat}(\vec{r}) = \frac{3\pi c^2}{2\hbar\omega_0^3}\left(\frac{\omega}{\omega_0}\right)^3\left(\frac{\Gamma}{\omega_0-\omega}+\frac{\Gamma}{\omega_0+\omega}\right)^2 I(\vec{r}) \tag{2.3}$$

A possible solution is the choice of a larger detuning $\Delta \equiv \omega_0 - \omega$, as the trap depth scales inversely proportional to Δ, the scattering rate however inversely proportional to Δ^2. This is the reason why most experiments with optical dipole traps operate at a large detuning of several THz.

2.1.2 Techniques to Control the Position and Motion of Atoms in a Cavity

In cavity QED with trapped atoms, the demonstration of new physical effects has often required an increase in control over the external degrees of freedom of the atoms. Therefore, the attempt to accurately localize an atom at a well-defined position in the cavity field and to eliminate its motion has a very long history. After the first successful trapping experiments [18], there have been numerous approaches to improve the localization and extend the storage times.

An early approach was to gain information about the atomic position and motion from the temporal modulation of a resonant laser beam transmitted through the cavity [16, 17]. Subsequent feedback onto the trap allowed to increase the atomic storage time [19]. With further improvement of the experimental setup and the electronics [20] and a higher output-coupling efficiency of the cavity, cooling of the atomic motion and storage times exceeding 1 s have been demonstrated [21].

The first QED experiments with second-long atom trapping times [22], however, used a different cooling method, namely a combination of red-detuned Doppler cooling (on a closed transition) and blue-detuned Sisyphus cooling (on another transition). In these experiments, Cs atoms were trapped in a magic-wavelength [11] FORT in a standing-wave configuration along the cavity axis. In search of faster cooling rates and lower temperatures, a mechanism has been proposed [23, 24] that directly makes use of the coupling to a cavity. The first implementation [25] of this cavity-cooling method used Rb atoms, also confined in an intra-cavity dipole trap.

The improved atom trapping in both of the above mentioned experimental setups led to the simultaneous achievement of another milestone in cavity QED—the observation of a normal mode spectrum with a single trapped atom [26, 27]. Achieving even longer atom trapping times was hampered by large parametric heating rates due to fluctuations of the used intra-cavity traps. This problem was avoided in a novel setup that used a cavity-independent FORT. With a combination of vacuum-stimulated and Sisyphus cooling, trapping times of 17 s were observed [28]. After replacement of the cavity and subsequent bake-out, this value was increased in the course of this thesis to more than 1 min on average [29], which is most likely limited by collisions with the background gas.

In addition to the increased storage times, the cavity-independent trap has another advantage: it allows to change the position of the atom along the beam axis with submicron precision [30] by shifting the standing-wave pattern of the trapping laser. This technique was later used in two different setups to deterministically transfer an atom to the cavity center [31, 32]. To this end, the exact number and position of atoms trapped in a standing-wave FORT has been determined with fluorescence imaging. Subsequently, the atoms were shifted to the center of a cavity using an optical conveyor belt [33]. In the experimental setup used in this thesis, this approach has been extended further. A high-numerical-aperture objective has been implemented which collects the light scattered by atoms trapped within the cavity mode [34]. Using the images of an electron-multiplying CCD camera then facilitates feedback onto

the position of the standing-wave trap [29], which allows us to localize the trapped atoms at a well-defined position within the cavity.

The above mentioned cooling mechanisms all lead to the observation of long storage times. However, it is also important to cool the atoms to a low temperature to avoid motion-induced dephasing, fluctuations in the atom-cavity coupling strength and a time-varying AC Stark shift of the atomic levels in case the trap is not a magic one [11]. In principle, cavity-cooling is a promising scheme for this purpose. With a long cavity of high finesse, even cooling below the recoil limit has been demonstrated with an atomic ensemble [35]. Unfortunately, cavity cooling requires the operation at a specific detuning, which prevents all experiments that operate at a different detuning or on resonance. The same holds for the recently proposed [36] and observed [37, 38] cavity EIT cooling. Therefore, the use of another technique is highly desirable. Along these lines, Raman sideband cooling—a very successful technique known from free-space experiments with trapped ions [9, 39, 40] and neutral atoms [41–46]—has been demonstrated in one dimension. Along the axis of the used intra-cavity dipole trap, the motional ground state has been achieved with a probability of 95 % [47].

To summarize, the control over motion and position of single atoms in cavity QED has been steadily improved over the past decades. In this thesis, this culminates in the achievement of full control, as explained in detail in Sect. 2.4. The decisive step towards this goal was the implementation of a three-dimensional optical lattice with high trap frequencies in all directions, described in Sect. 2.2. In addition, the current apparatus builds on many of the above mentioned techniques, especially on the use of a cavity-independent dipole trap with intra-cavity Sisyphus cooling [28] and Raman sideband cooling [47], a blue-detuned intra-cavity trap [48], imaging [34] and active atom positioning [30, 33]. As a side remark, these techniques and the increasing experimental complexity have raised the demands on the stability of the setup. Therefore, literally every part of the laser system, the optics setup and the frequency stabilization electronics has been replaced and rebuilt in the course of this thesis.

2.2 Implementation of a 3D Optical Lattice in a Cavity

Previous approaches to atom trapping in a cavity used only one retro-reflected laser beam, as described in 2.1.2. This only provides subwavelength confinement in the direction of the standing-wave pattern, i.e. along the laser beam axis, which leads to several experimental drawbacks. First, even at low temperatures, the residual atomic motion is usually on a scale that is comparable to the wavelength of the used lasers. This prevents all experiments that require phase-stable illumination of the atom. When the trap axis does not coincide with that of the resonator, the atomic motion also poses the problem of strongly fluctuating atom-cavity coupling strength. In addition, the trap frequencies in the orthogonal directions are comparably small,

typically on the order of a few kHz. This can be the cause of reduced atom trapping times due to parametric heating, caused by acoustic vibrations of the optics setup in this frequency regime.

In this thesis, the aforementioned obstacles have been eliminated by implementing a 3D optical lattice within the cavity. The trapping geometry has been designed such that the atoms can be deterministically located at the maximum of the intra-cavity field to achieve the maximum possible coupling strength. This is especially challenging along the axis of the resonator, where the cavity mode exhibits a standing-wave structure and the atoms thus have to be localized with subwavelength precision. Therefore, one of the axes of the optical lattice has been chosen to coincide with the cavity axis. In this configuration, the standing-wave structure of the cavity and that of the lattice always exhibit a fixed spatial relation. In addition, the reflection or the transmission of the trapping laser can be used to derive an error signal that allows to stabilize the cavity resonance frequency with the Pound-Drever-Hall technique [49].

Unfortunately, due to the AC Stark shift induced by the trap light, this geometry can also have two severe drawbacks: First, fluctuations of the cavity length, e.g. due to uncompensated mechanical vibrations, will affect the intensity of the trap laser and thus lead to fluctuating atomic transition frequencies. Second, circular polarization components of the trap can arise from cavity birefringence. This leads to differential shifts of the atomic ground states and thus to decoherence of superposition states when the intensity fluctuates or the atoms move in the trap. Both problems can be minimized by using a blue-detuned lattice beam along the cavity axis. In this case, cold atoms are trapped at a node of the field, such that they experience low absolute AC Stark shifts even at high trap intensities. With respect to the absolute value of the trap laser detuning, one has to consider the beating pattern between the blue-detuned trap and the intra-cavity field at the atomic resonance frequency, which can be seen in Fig. 2.2a. When the relative detuning corresponds to an odd number of free spectral ranges, a maximum of the intra-cavity field (red) will coincide at the center of the resonator with a minimum of the trapping potential (blue), such that the atom (black dot) is trapped at a position with maximum coupling strength. In the experiments described in this thesis, the blue-detuned trap was operated at a wavelength of 771 nm, which leads to a beating period of about 32 µm, which poses only moderate requirements on the accuracy of the atom positioning.

In contrast to the trap along the cavity axis, the lattice beams along the orthogonal directions can be implemented with a high degree of experimental flexibility. In the existing setup, the use of a horizontally and a vertically oriented trap seemed to be favorable in terms of optical access. We chose to use a blue-detuned (771 nm) and a red detuned (1064 nm) laser beam. The resulting configuration is illustrated in Fig. 2.2b (not to scale). Before the laser setup is explained in more detail, the reasons for the used wavelength configuration are presented in the following.

There are two major advantages of using a blue-detuned trap along the vertical axis: First, at low temperatures the scattering-induced heating rate of a blue trap is smaller than that of a red trap at the same detuning [10]. Second, the atoms are trapped at an antinode of the standing wave, which means that the AC Stark shift is close to zero, independent of the exact intensity of the trap light. Therefore, the

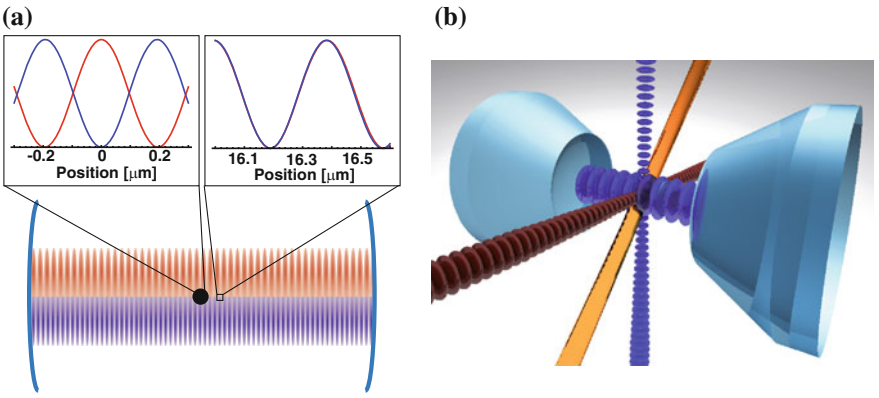

Fig. 2.2 **a** Spatial structure of the intra-cavity dipole trap (not to scale). The atom (*black dot*) is trapped in a blue-detuned standing-wave trap (*blue*) which has a different wavelength than the cavity mode (*red*). Thus, the atom-cavity coupling depends on the atomic position along the resonator axis. This is indicated in the plots above. When the atom is trapped at the center of the resonator (0 μm, *left*), it experiences the maximum coupling strength, while the coupling is very small when the atom is trapped at a position 16 μm away from the center (*right*), such that the cavity mode and the trap light largely overlap. **b** Sketch of the setup geometry (not to scale). The atoms are trapped at the center of a resonator that is made of two highly-reflective spherical mirrors (*light blue*), which are coned to provide better optical access. The atoms are trapped in a three-dimensional optical lattice which consists of three orthogonal standing-wave fields, one red-detuned (along the horizontal axis) and two blue-detuned. The atoms can be addressed with laser beams of different frequencies that impinge either along the cavity axis or from the side (*orange*), oriented perpendicular to the cavity axis and at an angle of 45° with respect to the other trapping beams

frequencies of the atomic transitions remain constant, even if the spatial position of the laser beams that form the 3D optical lattice drifts over time.

For the horizontal axis, however, we chose to employ a red-detuned laser beam operating at 1064 nm. This also has several advantages: First, the attractive potential of the resulting standing-wave trap allows to efficiently load atoms into the lattice [50]. Second, this wavelength has proven to facilitate efficient cooling of the trapped atoms using a Sisyphus-like mechanism [28]. Third, the atoms are trapped at a position of maximum intensity. When the trap light is linearly polarized along the quantization axis, this leads to a Zeeman-state dependent level splitting of the excited state (described in more detail in Sect. 3.1, see Fig. 3.1), which has proven useful for efficient optical pumping [51] and for the implementation of the quantum gate described in Chap. 6 without an interferometrically stable optics setup. However, the use of a red detuned trap also has a caveat: It is very important that the trap light does not exhibit any circular polarization components, as they would lead to considerable differential AC Stark shifts of the ground-state Zeeman levels. This could lead to a severe reduction in coherence time if the atom is moving in the trap or if the trap intensity fluctuates.

In the following, the laser setup of both traps is explained in more detail, starting with the red-detuned one. The previously existing setup of this trap [52] had used electro-optical modulators for the required trap switching. These modulators, however, turned out to be very unstable with respect to thermal fluctuations and have therefore been replaced with AOMs. In addition, optical fibers have been introduced into the beam path to improve the spatial profile of the trapping beam and to reduce the sensitivity of the setup with respect to temperature fluctuations. In order to ensure that the trap light does not exhibit any circular polarization components, a Semrock polarizing bandpass filter is used. This yields a measured polarization extinction ratio of $10^6 : 1$, which is an improvement by three orders of magnitude compared to the previous setup. Apart from these modifications, the geometry is described in the thesis of Stephan Nußmann [50].

In the following, the setup of the vertical trap is explained. The lattice beam originates from the same laser as that of the intra-cavity trap. To prevent any interference effects, the polarization of both beams is set orthogonal. In addition, they are detuned by several hundred MHz with respect to each other, such that a possibly remaining interference pattern is averaged out as it changes on a timescale that is fast compared to the atomic motion. The laser beam impinges to the vacuum chamber from the bottom, meaning that all optics can be placed close to the surface of the optical table, where a stable mounting is guaranteed. The beam is focused to the atoms with an achromatic doublet lens of 2.5 cm focal length, leading to a diffraction-limited spot size of about 10 µm (FWHM) at the focal position. After passing through the vacuum chamber, the beam is collimated by the same objective that is also used to image the atoms. This objective was designed by A. Kochanke and provides a nearly diffraction-limited resolution at the two design wavelengths 780 and 1064 nm. The 771 nm trapping light is retro-reflected after separation from the atomic fluorescence with several bandpass filters.

The fluorescence light is focused onto an electron-multiplying CCD camera, which allows to record the atom distribution with up to five images per second. Figure 2.3 shows two typical images, one with the intracavity trap switched off (left), and one in the 3D-lattice configuration (right). The tighter confinement of the atom can be directly seen, as its size is clearly reduced in the vertical direction in the image, which corresponds to the cavity axis.

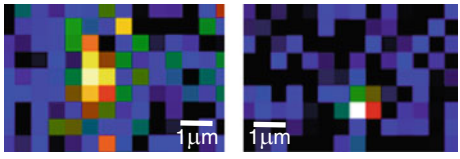

Fig. 2.3 Fluorescence images of single trapped atoms with the intra-cavity trap switched off (*left*) or on (*right*), respectively. The presence of the confining potential can be seen directly in the images, as it reduces the atomic extent along the vertical axis in the images, which corresponds to the cavity axis. The color scale is linear, normalized to the highest intensity value of each image

2.3 Deterministic Localization of a Single Atom at the Center of the Resonator

In the following section, the techniques to localize an atom at a predefined position in the resonator are explained. The contents of this section have been published in [53]: *Ground-State Cooling of a Single Atom at the Center of an Optical Cavity*. A. Reiserer, C. Nölleke, S. Ritter, G. Rempe. Physical Review Letters **110**, 223003 (2013).

In our setup, each experimental run starts with the preparation of a cloud of ^{87}Rb atoms in a magneto-optical trap (MOT). To transfer the atoms to the optical resonator, a running-wave dipole trap is then used. When the atoms arrive in the cavity, they are first loaded into the red-detuned 1D optical lattice using the procedure described in [30, 50]. Subsequently, cooling light is applied in a counter-propagating geometry from the side of the resonator (orange laser beam in Fig. 2.2). The cooling light is 30 MHz red-detuned with respect to the $F = 2 \leftrightarrow F' = 3$ transition of the D_2 line and has orthogonal linear polarizations, which leads to cooling of the atom in all three dimensions using a Sisyphus-type mechanism [28, 50]. A high numerical aperture objective is used to collect light that is scattered by the atom, which allows to image the atoms and to determine their number and position using an algorithm that evaluates the recorded intensity pattern. The loading procedure is repeated until a single atom is detected in the images [54]. Subsequently, the standing-wave pattern is shifted along the beam, which allows to deterministically transfer the atom to an arbitrary position within the cavity mode [30]. Subsequently, the lattice beams described in Sect. 2.2 are switched on, such that the atom is tightly confined along all directions.

In the following, experimental control of the coupling strength is demonstrated by loading the atoms at different positions with respect to the cavity field. We measure the transmission of a weak probe laser pulse, which is resonant with the empty cavity and the Stark-shifted atomic transition from $|F, m_F\rangle = |2, 2\rangle$ to $|3, 3\rangle$. Here, F denotes the atomic hyperfine state and m_F its projection onto the quantization axis, which coincides with the cavity axis. Depending on the coupling strength, the transmission is suppressed, as explained in Sect. 1.2. Shifting the atom along the axis of the red detuned trap therefore gives a Gaussian dependence (red dots in Fig. 2.4a), due to the Gaussian radial profile of the cavity mode. When shifting the red-detuned dipole trap along the cavity axis (using a piezo mirror), a beating between the sinusoidal variation of the effective coupling strength g and the standing-wave trap along the cavity axis is expected, see Fig. 2.2a and [12, 13, 55]. This is shown in Fig. 2.4a (black squares).

We observe a sinusoidal modulation of the transmission. The deviation from the ideally expected oscillation with the same period but steeper slopes is caused by a position-dependent optical pumping efficiency and temperature, which leads to averaging effects in coupling strength and Stark shift. Due to the loading procedure, the

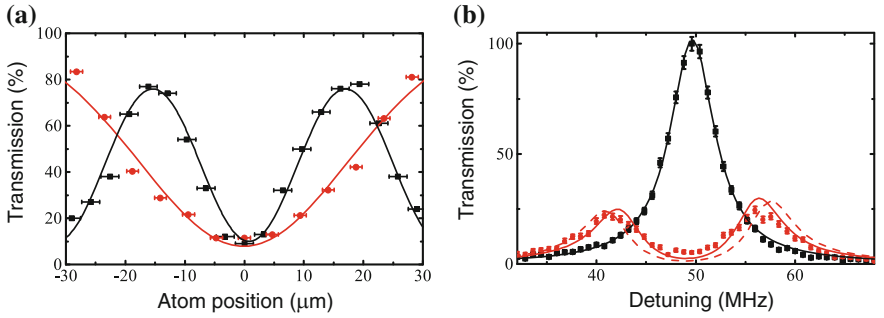

Fig. 2.4 **a** Transmission through the cavity when the position of a single, coupled atom is scanned along the cavity axis (*black squares*) and along an orthogonal axis (*red dots*). The transmission is strongly suppressed when the atom is located at a maximum of the intracavity field. The solid Gaussian (*red*) and sine (*black*) fit curves are a guide for the eye. **b** Normal-mode spectroscopy of the atom-cavity system with the atom trapped in the 3D optical lattice. The transmission of the cavity is a Lorentzian curve when the atom is not coupled (*black squares* and *black fit curve*), while a resonant atom leads to a normal-mode splitting (*red dots* and *solid red fit curve*). The slight asymmetry is caused by a small residual detuning between atom and cavity. The error bars are statistical. The dashed curve shows the spectrum expected for $g_0/2\pi = 8\,\text{MHz}$, the value calculated from our cavity parameters (from [53])

initial distribution of the atoms in the lattice is determined by their initial temperature and the beam waist of the red-detuned dipole trap. We determine the width of this distribution from the fluorescence images. This gives the error bars in Fig. 2.4a. On the length scale of the positioning error, the transmission is nearly constant. We can thus deterministically localize a single atom at the maximum of the resonator field, where the atom-cavity coupling is strongest.

The absolute strength of this coupling is determined by recording the normal-mode spectrum of the atom-cavity system [2]. To this end, the frequency of the probe laser is scanned while the frequency of the cavity is kept fixed. To record the spectrum of the empty cavity, the atom is first pumped to $F = 1$ such that it is not coupled to the resonator. Thus, the transmission is a Lorentzian curve with a full width at half maximum of 5.5 MHz (Fig. 2.4b, black squares). When the atom is prepared in the $|2, 2\rangle$ state, we observe a normal-mode splitting (red dots). The separation of the two peaks is twice the atom-cavity coupling constant g. To determine this value, we fit the normal modes with a theory curve (solid red line) with g and the atomic detuning as the only free parameters. From this fit, we find $g/2\pi = (6.7 \pm 0.1)\,\text{MHz}$, close to the theoretical value of $g_0/2\pi = 8\,\text{MHz}$ (dashed red line). This again proves that we are able to accurately localize the atom at the center of the cavity field and that the system is in the single-atom strong coupling regime of CQED.

2.4 Sideband Spectroscopy and Ground-State Cooling

In Sect. 2.3, excellent control over the position of a single atom with respect to the cavity mode has been demonstrated. This section will present techniques to control its motion. Again, the contents of this section have partially been published in [53].

In the implemented optical lattice (see Sect. 2.2), the atom is tightly confined in all three dimensions to a spatial extent that is small compared to the wavelength of the employed optical transitions (spatial extent of the ground-state wave function $\lesssim$15 nm). This situation is called the Lamb-Dicke regime, in which very powerful techniques to analyze and control the atomic motion exist. These techniques have been pioneered in free space experiments with single trapped ions [9, 40] and ensembles of neutral atoms [10, 56, 57]. Recently, they have been applied to single neutral atoms trapped in optical tweezers [45, 46] and—in this thesis—in a three-dimensional optical lattice. The basic idea is that two Raman laser beams allow one to drive transitions between the different motional states of the atom. While the used setup will be described in more detail in Sect. 3.2, this section will focus on its application to atom cooling.

In our experiment, the atom is trapped in a three-dimensional optical lattice at a temperature that is small compared to the trap depth. Thus, the confining potential can be well approximated by a three-dimensional harmonic potential, as explained in more detail in Sect. 2.1.1. In this situation, the atomic motion is quantized with equally spaced energy levels with $E = (n + \frac{1}{2}) \cdot h\nu_{trap}$ [10]. A pair of Raman lasers is employed, which exhibit a relative detuning that equals the hyperfine splitting of 6.8 GHz and a common detuning of 0.3 THz with respect to the D_1 line at 795 nm. Because of this large detuning, the Raman beams lead to an effective coupling of the two hyperfine ground states without populating the excited state. The linewidth of this coupling can be much smaller than the natural linewidth of the D_1 transition. This allows one to drive atomic transitions that increase or lower the vibrational quantum number n, as schematically depicted in Fig. 2.5a. The coupling strength of these transitions is given by the following formulas [9]:

$$\begin{aligned} \Omega_{n\to n-1} &= \Omega_{n\to n}\eta\sqrt{n} \\ \Omega_{n\to n+1} &= \Omega_{n\to n}\eta\sqrt{n+1} \end{aligned} \tag{2.4}$$

Here, $\Omega_{n\to n}$ denotes the Rabi frequency of the carrier transition, which depends on the geometry, polarization and intensity of the used laser beams. $\Omega_{n\to n-1}$ ($\Omega_{n\to n+1}$) is the Rabi frequency of a transition on the red (blue) sideband, which lowers (increases) the vibrational quantum number by one. $\eta = \sqrt{\frac{\hbar}{4\pi m\nu_{trap,x}}}\Delta k_x$ is called the Lamb-Dicke parameter, which depends on the atomic mass m and Δk_x, the wavevector difference of the two Raman laser beams, projected onto the axis of motion $\vec{x}$. In our experiment, $\eta \simeq 0.1$. From Eq. (2.4), one can directly see that the coupling strength of the sideband transitions depends on the vibrational quantum number n. When R

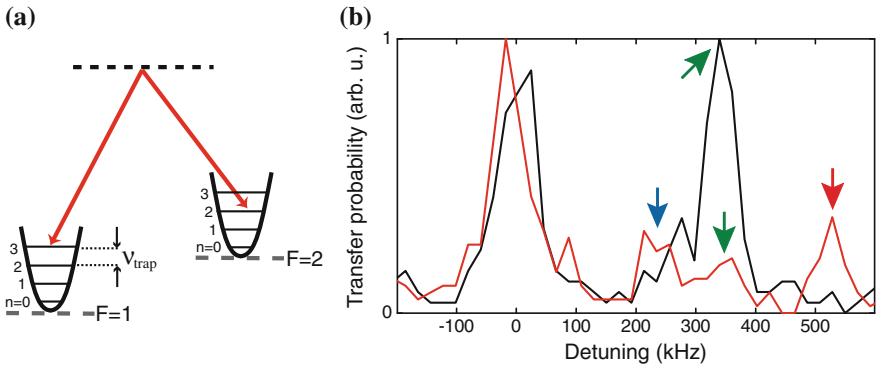

Fig. 2.5 **a** Coupling of different motional states with Raman lasers. The atom is confined in a harmonic potential, which is schematically depicted for the two ground states $F = 1$ and $F = 2$. With the right detuning of the Raman laser beams (*red arrows*), states with different vibrational quantum number can be coupled. **b** Amplitude of the Raman carrier and the blue sideband. When the atom is trapped at the center of the cavity (*black line*), only the central sideband (*green arrow*) that corresponds to the trap along the cavity axis is resolved. When the atomic position is shifted by ∼5 µm (*red line*) by shifting the red-detuned trap, all three sidebands are visible with comparable height (colored arrows; *blue* vertical axis; *green* cavity axis; *red* horizontal axis)

denotes the ratio of the transition probabilities on the red and blue sidebands, the average vibrational quantum number $\bar{n}$ of a thermal state is given by [9]:

$$\bar{n} = \frac{R}{1 - R} \tag{2.5}$$

Thus, it is possible to determine the atomic temperature when the sidebands can be resolved in a spectroscopic measurement. To experimentally obtain a sideband spectrum, the atom is optically pumped to the $F = 1$ hyperfine state. Subsequently, the Raman lasers are applied for a certain time period, typically 200 µs. In order to measure the population transfer to $F = 2$, cavity-based hyperfine state detection is employed [54], which will be described in more detail in Sect. 3.1.

To analyze and control the atomic motion, we first used a geometry where one of the beams was applied along the cavity, while the other beam was applied from the side, forming an angle of 45° with respect to the other axes of the optical lattice, compare Fig. 2.2b. The beams were orthogonally polarized, thus driving transitions for any of the atomic Zeeman states. However, it turned out that in this configuration, the coupling strength of the individual sidebands strongly depends on the atomic position within the standing-wave Raman beam, similar to what has been observed in [47]. The reason is that the standing-wave Raman field has a fixed phase of α with respect to the intracavity trap, which yields $\Omega^{\text{intracavity}}_{n\rightarrow n\pm1} = \Omega_{n\rightarrow n\pm1} \sin(2\alpha)$ [47]. This effect is not present for the orthogonal axes, where the Raman beams do not exhibit a standing-wave structure. Due to the change in α, the relative amplitude of the intracavity sideband with respect to those of the other axes changes when the

atom is trapped at different positions along the resonator axis. This effect can be seen in the sideband spectrum of Fig. 2.5b. When the atom is trapped at the center of the cavity (black line), the sidebands of the orthogonal traps are much smaller than that of the intracavity trap (green arrow), while they can be clearly resolved (blue and red arrow) when the atomic position is shifted by ∼5 μm (red line) along the cavity axis.

In order to cool the atom in all three dimensions at the center of the cavity, however, it is highly advantageous to have equal coupling strengths on all three sidebands. Therefore, an additional Raman laser beam is employed, which is counter-propagating to the beam that is applied from the side. Its polarization is set orthogonal to both other beams to prevent interference effects. It drives transitions on all sidebands except that along the cavity axis. Thus, the relative amplitude of the other sidebands can be increased with the power in the additional Raman beam. With this, the amplitude of all three sidebands is in the following set to a comparable height, and the atomic temperature after intra-cavity Sisyphus cooling is investigated.

The green line in Fig. 2.6a shows an obtained sideband spectrum, where zero detuning means a frequency difference that corresponds to the hyperfine transition frequency. The large peak at the center of the spectrum is the saturated carrier transition. At negative detunings, the red sidebands can be seen, corresponding to transitions that lower the vibrational state of the atom by one quantum. The three peaks at positive detunings correspond to the blue sideband for each of the three lattice axes: the red-detuned dipole trap (at 0.5 MHz) and the blue-detuned traps along the vertical axis (0.4 MHz) and along the cavity axis (0.3 MHz). The peaks can be identified unambiguously by successively changing the intensity of one of the lattice beams and then recording the sideband spectrum (not shown). The central sideband peak

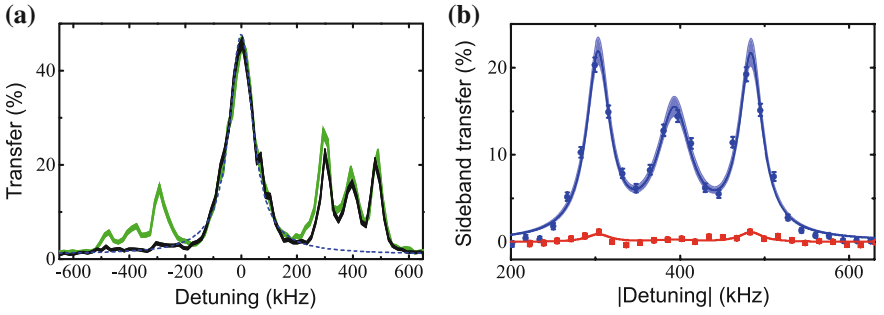

Fig. 2.6 **a** Sideband spectrum after intra-cavity Sisyphus (*green*) and after sideband cooling (*black*). The statistical standard error of the data is given by the thickness of the lines. The *three peaks* at positive detunings correspond to a transition on the blue sideband for each axis of the 3D lattice potential (*right* to *left*: $\hat{x}$, $\hat{y}$, $\hat{z}$ axis). The carrier peak at the center (*dashed blue* Lorentzian fit curve) is saturated. Transitions on the red sideband (negative detunings) are still observed after Sisyphus cooling (*green*) but nearly vanish after 5 ms of sideband cooling (*black*). **b** Transfer probability on the red (*red squares*) and blue (*blue dots*) sideband after Raman sideband cooling. The solid curves are numerical fits of the sum of three Lorentzian curves, with the *shaded areas* indicating the 66 % confidence interval. The atomic temperature after sideband cooling is determined from these fits (from [53])

is lower and broader than the other two in the depicted long-term measurement. On shorter timescales, three peaks of the same height are observed, but with fluctuating position of the central peak. This is caused by long-term drifts in beam pointing, as at the time of the depicted measurement a lattice beam with a much tighter focus was used along the vertical axis due to the limited laser power available. Meanwhile, this laser has been replaced by one that gives a much higher output power, and the spot size has been doubled to reduce the trap-frequency fluctuations.

Applying (2.5) to a fit of the green curve in Fig. 2.6a gives $\bar{n}_{\{x,y,z\}} = \{0.19(5), 0.4(1), 1.0(2)\}$. Here, x corresponds to the axis of the red-detuned trap, y to the vertical and z to the cavity axis. This demonstrates that the intra-cavity Sisyphus cooling mechanism already leads to temperatures well below the Doppler limit [28, 50] ($\bar{n}_D \approx 6$–10 for our trap frequencies). To further reduce the atomic temperature, pulsed Raman sideband cooling is used. To this end, the atom is prepared in $F = 1$ and the Raman beams are applied for 5 ms with frequency components that drive transitions on all three red sidebands. During this interval, a $\approx$10 ns long repump pulse is applied on the $F = 2 \leftrightarrow F' = 1$ transition every 200 ns in order to bring any transferred population back to $F = 1$ where the cooling cycle can start again. To determine the effect of the sideband cooling, the following measurement cycle is performed: First, a 4.4 ms long interval of intra-cavity Sisyphus cooling is applied on the closed transition. Then, the transfer probability at a certain Raman detuning is recorded. Subsequently, sideband cooling is applied and the transfer probability at the same detuning is measured again. This measurement sequence is repeated at different frequencies to record a spectrum immediately before (green in Fig. 2.6a) and after (black) sideband cooling. The red sidebands vanish almost completely, which indicates that the atom is cooled close to the ground state.

To determine the mean occupation number $\bar{n}$, a Lorentzian curve is fit to the carrier (blue dashed line in Fig. 2.6a) and subtracted from the data (Fig. 2.6b). Subsequently, the sum of three Lorentzian curves is fit to the blue sidebands (blue curve) to determine the width and frequency of the three peaks as well as their respective amplitudes. Using the same frequencies and widths for the red sidebands, their amplitude is determined, again from a least-squares fit to the data (red curve). This gives $\bar{n}_{\{x,y,z\}} = \{0.04(1), 0.02(1), 0.06(1)\}$. Assuming a thermal distribution, this means that the atom is cooled to the 1D ground state with a probability of $\{0.96(1), 0.98(1), 0.95(1)\}$ and to the 3D ground state with a probability of (89 ± 2) %.

One of the main advantages of cooling to low temperatures is that the atomic transition frequencies are expected to be constant, even without the use of a trap at a magic wavelength [11]. To investigate whether this is the case in our experimental setup, we perform a measurement of the AC Stark shift. To this end, the atom is prepared in $F = 1$ and a laser resonant with the transition to $\left|1', \pm 1\right\rangle$ is irradiated. The frequency of this transfer laser is scanned and the transfer probability to $F = 2$ is measured, conditioned on atom trapping at the center of the red-detuned dipole trap using the camera images. This gives the spectrum in Fig. 2.7. While this measurement was performed after ground-state cooling, a similar result can be obtained in the 3D lattice using only intra-cavity Sisyphus cooling (not shown), as this already leads to sufficiently low temperatures (as demonstrated above).

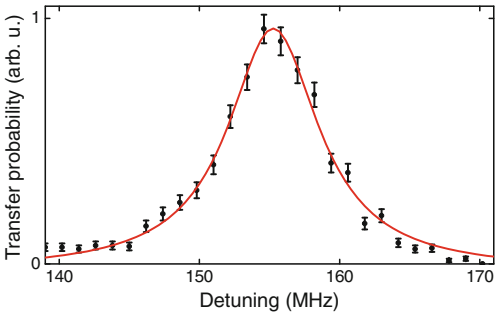

Fig. 2.7 AC Stark shift of the atomic transition after cooling the atom to the three-dimensional motional ground state. The measured linewidth (*red Lorentzian fit curve*) is 8 MHz FWHM, close to the natural linewidth of the atomic transition (6 MHz). The remaining broadening is due to atom trapping at different positions within the red-detuned dipole trap, which are not resolved in the camera images. The *error bars* denote the standard error of the mean

The observed spectrum has a Lorentzian linewidth of 8 MHz (FWHM) (red fit curve), which is slightly broader than the natural linewidth of the atomic transition (6 MHz). The remaining deviation is caused by different atom-trapping positions in the lattice, which are not resolved in the camera images, but can still lead to a slightly different intensity of the 1064 nm light. Without conditioning on the atom position, a larger linewidth of about 12 MHz is observed. Still, this value constitutes some improvement compared to previous experiments in our setup, where a typical value of 23 MHz (FWHM) was observed [52]. This improvement was a prerequisite for the observation of a clear normal-mode splitting [53] (see Sect. 2.4) and thus for the experiments presented in Chaps. 5 and 6 [58, 59].

References

1. G. Rempe et al., Optical bistability and photon statistics in cavity quantum electrodynamics. Phys. Rev. Lett. **67**(13), 1727–1730 (1991). doi:10.1103/PhysRevLett.67.1727. http://link.aps.org/doi/10.1103/PhysRevLett.67.1727
2. R.J. Thompson, G. Rempe, H.J. Kimble, Observation of normal-mode splitting for an atom in an optical cavity. Phys. Rev. Lett. **68**(8), 1132–1135 (1992). 00722, doi:10.1103/PhysRevLett.68.1132. http://link.aps.org/doi/10.1103/PhysRevLett.68.1132
3. Q.A. Turchette et al., Measurement of conditional phase shifts for quantum logic. Phys. Rev. Lett. **75**(25), 4710–4713 (1995). doi:10.1103/PhysRevLett.75.4710. http://link.aps.org/doi/10.1103/PhysRevLett.75.4710
4. J. Harold, in *Metcalf and Peter Van der Straten*. Laser Cooling And Trapping, (Springer, 1999). ISBN: 978-0-387-98728-6
5. C.J. Hood et al., Real-time cavity QED with single atoms. Phys. Rev. Lett. **80**(19), 4157–4160 (1998). doi:10.1103/PhysRevLett.80.4157. http://link.aps.org/doi/10.1103/PhysRevLett.80.4157
6. M. Hennrich et al., Vacuum-stimulated raman scattering based on adiabatic passage in a high-finesse optical cavity. Phys. Rev. Lett. **85**(23), 4872–4875 (2000). doi:10.1103/PhysRevLett.85.4872. http://link.aps.org/doi/10.1103/PhysRevLett.85.4872

7. P. Münstermann et al., Dynamics of single-atom motion observed in a high-finesse cavity. Phys. Rev. Lett. **82**(19), 3791–3794 (1999). doi:10.1103/PhysRevLett.82.3791. http://link.aps.org/doi/10.1103/PhysRevLett.82.3791
8. P. Münstermann et al., Observation of cavity-mediated long-range light forces between strongly coupled atoms. Phys. Rev. Lett. **84**(18), 4068–4071 (2000). doi:10.1103/PhysRevLett.84.4068. http://link.aps.org/doi/10.1103/PhysRevLett.84.4068
9. D. Leibfried et al., Quantum dynamics of single trapped ions. Rev. Mod. Phys. **75**(1), 281 (2003). doi:10.1103/RevModPhys.75.281. http://link.aps.org/doi/10.1103/RevModPhys.75.281
10. R. Grimm, M. Weidemüller, Y.B. Ovchinnikov, Optical dipole traps for neutral atoms. Adv. At. Mol. Opt. Phys. **42**, 95–170 (Academic Press, 2000). ISBN: 978-0-12-003842-8. http://www.sciencedirect.com/science/article/pii/S1049250X0860186X
11. A. Derevianko, H. Katori, Colloquium: physics of optical lattice clocks. Rev. Mod. Phys. **83**(2), 331–347 (2011). doi:10.1103/RevModPhys.83.331. http://link.aps.org/doi/10.1103/RevModPhys.83.331
12. G.R. Guthöhrlein et al., A single ion as a nanoscopic probe of an optical field. Nature **414**(6859), 49–51 (2001). ISSN: 0028-0836. doi:10.1038/35102129. http://www.nature.com/nature/journal/v414/n6859/abs/414049a0.html
13. A.B. Mundt et al., Coupling a single atomic quantum bit to a high finesse optical cavity. Phys. Rev. Lett. **89**(10), 103001 (2002). 00291, doi:10.1103/PhysRevLett.89.103001. http://link.aps.org/doi/10.1103/PhysRevLett.89.103001
14. D. Hunger et al., A fiber Fabry-Perot cavity with high finesse. New J. Phys. **12**(6), 065038 (2010). ISSN: 1367–2630. doi:10.1088/1367-2630/12/6/065038. http://iopscience.iop.org/1367-2630/12/6/065038
15. M. Steiner et al., Single ion coupled to an optical fiber cavity. Phys. Rev. Lett. **110**(4), 043003 (2013). 00015, doi:10.1103/PhysRevLett.110.043003. http://link.aps.org/doi/10.1103/PhysRevLett.110.043003
16. C.J. Hood et al., The atom-cavity microscope: single atoms bound in orbit by single photons. Science **287**(5457), 1447–1453 (2000). ISSN: 0036-8075, 1095-9203. doi:10.1126/science.287.5457.1447. http://www.sciencemag.org/content/287/5457/1447
17. P.W.H. Pinkse et al., Trapping an atom with single photons. Nature **404**(6776), 365–368 (2000). ISSN: 0028-0836. doi:10.1038/35006006. http://dx.doi.org/10.1038/35006006
18. J. Ye, D.W. Vernooy, H.J. Kimble, Trapping of single atoms in cavity QED. Phys. Rev. Lett. **83**(24), 4987–4990 (1999). doi:10.1103/PhysRevLett.83.4987. http://link.aps.org/doi/10.1103/PhysRevLett.83.4987
19. T. Fischer et al., Feedback on the motion of a single atom in an optical cavity. Phys. Rev. Lett. **88**(16), 163002 (2002). 00106, doi:10.1103/PhysRevLett.88.163002. http://link.aps.org/doi/10.1103/PhysRevLett.88.163002
20. A. Kubanek et al., Photon-by-photon feedback control of a single-atom trajectory. Nature **462**(7275), 898–901 (2009). ISSN: 0028-0836. doi:10.1038/nature08563. http://dx.doi.org/10.1038/nature08563
21. M. Koch et al., Feedback cooling of a single neutral atom. Phys. Rev. Lett. **105**(17), 173003 (2010). 00034, doi:10.1103/PhysRevLett.105.173003. http://link.aps.org/doi/10.1103/PhysRevLett.105.173003
22. J. McKeever et al., State-insensitive cooling and trapping of single atoms in an optical cavity. Phys. Rev. Lett. **90**(13), 133602 (2003). 00324, doi:10.1103/PhysRevLett.90.133602. http://link.aps.org/doi/10.1103/PhysRevLett.90.133602
23. P. Horak et al., Cavity-induced atom cooling in the strong coupling regime. Phys. Rev. Lett. **79**(25), 4974–4977 (1997). 00252, doi:10.1103/PhysRevLett.79.4974. http://link.aps.org/doi/10.1103/PhysRevLett.79.4974
24. V. Vuletic, S. Chu, Laser cooling of atoms, ions, or molecules by coherent scattering. Phys. Rev. Lett. **84**(17), 3787–3790 (2000). 00259, doi:10.1103/PhysRevLett.84.3787. http://link.aps.org/doi/10.1103/PhysRevLett.84.3787

25. P. Maunz et al., Cavity cooling of a single atom. Nature **428**(6978), 50–52 (2004). ISSN: 0028-0836. doi:10.1038/nature02387. http://dx.doi.org/10.1038/nature02387
26. A. Boca et al., Observation of the vacuum rabi spectrum for one trapped atom. Phys. Rev. Lett. **93**(23), 233603 (2004). doi:10.1103/PhysRevLett.93.233603. http://link.aps.org/doi/10.1103/PhysRevLett.93.233603
27. P. Maunz et al., Normal-mode spectroscopy of a single-bound-atom-cavity system. Phys. Rev. Lett. **94**(3), 033002 (2005). doi:10.1103/PhysRevLett.94.033002. http://link.aps.org/doi/10.1103/PhysRevLett.94.033002
28. S. Nußmann et al., Vacuum-stimulated cooling of single atoms in three dimensions. Nat. Phys. **1**(2), 122–125 (2005). ISSN: 1745-2473. doi:10.1038/nphys120. http://www.nature.com/nphys/journal/v1/n2/abs/nphys120.html
29. H.P. Specht et al., A single-atom quantum memory. Nature **473**(7346), 190–193 (2011). 00128, ISSN: 0028-0836. doi:10.1038/nature09997. http://dx.doi.org/10.1038/nature09997
30. S. Nußmann et al., Submicron positioning of single atoms in a microcavity. Phys. Rev. Lett. **95**(17), 173602 (2005). doi:10.1103/PhysRevLett.95.173602. http://link.aps.org/doi/10.1103/PhysRevLett.95.173602
31. K.M. Fortier et al., Deterministic loading of individual atoms to a high-finesse optical cavity. Phys. Rev. Lett. **98**(23), 233601 (2007). doi:10.1103/PhysRevLett.98.233601. http://link.aps.org/doi/10.1103/PhysRevLett.98.233601
32. M. Khudaverdyan et al., Controlled insertion and retrieval of atoms coupled to a high-finesse optical resonator. New J. Phys. **10**(7), 073023 (2008). 00053, ISSN: 1367-2630. doi:10.1088/1367-2630/10/7/073023. http://iopscience.iop.org/1367-2630/10/7/073023
33. S. Kuhr et al., Deterministic delivery of a single atom". Science **293**(5528), 278–280 (2001). ISSN: 0036-8075, 1095-9203. doi:10.1126/science.1062725. http://www.sciencemag.org/content/293/5528/278
34. B. Weber et al., Photon-photon entanglement with a single trapped atom. Phys. Rev. Lett. **102**(3), 030501 (2009). 00082, doi:10.1103/PhysRevLett.102.030501. http://link.aps.org/doi/10.1103/PhysRevLett.102.030501
35. M. Wolke et al., Cavity cooling below the recoil limit. Science **337**(6090), 75–78 (2012). 00027, ISSN: 0036-8075, 1095-9203. doi:10.1126/science.1219166. http://www.sciencemag.org/content/337/6090/75
36. M. Bienert, G. Morigi, Cavity cooling of a trapped atom using electromagnetically induced transparency. New J. Phys. **14**(2), 023002 (2012). 00016, ISSN: 1367-2630. doi:10.1088/1367-2630/14/2/023002. http://iopscience.iop.org/1367-2630/14/2/023002
37. T. Kampschulte et al., Optical control of the refractive index of a single atom. Phys. Rev. Lett. **105**(15), 153603 (2010). 00067, doi:10.1103/PhysRevLett.105.153603. http://link.aps.org/doi/10.1103/PhysRevLett.105.153603
38. T. Kampschulte et al., Electromagnetically-induced-transparency control of single-atom motion in an optical cavity. Phys. Rev. A **89**(3), 033404 (2014). 00000, doi:10.1103/PhysRevA.89.033404. http://link.aps.org/doi/10.1103/PhysRevA.89.033404
39. F. Diedrich et al., Laser cooling to the zero-point energy of motion. Phys. Rev. Lett. **62**(4), 403–406 (1989). 00693, doi:10.1103/PhysRevLett.62.403. http://link.aps.org/doi/10.1103/PhysRevLett.62.403
40. C. Monroe et al., Resolved-sideband Raman cooling of a bound atom to the 3d zero-point energy. Phys. Rev. Lett. **75**(22), 4011–4014 (1995), doi:10.1103/PhysRevLett.75.4011. http://link.aps.org/doi/10.1103/PhysRevLett.75.4011
41. H.J. Lee et al., Raman cooling of atoms in an optical dipole trap. Phys. Rev. Lett. **76**(15), 2658 (1996), doi:10.1103/PhysRevLett.76.2658. http://link.aps.org/doi/10.1103/PhysRevLett.76.2658
42. V. Vuletic et al., Degenerate Raman sideband cooling of trapped cesium atoms at very high atomic densities. Phys. Rev. Lett. **81**(26), 5768–5771 (1998). 00210. doi:10.1103/PhysRevLett.81.5768. http://link.aps.org/doi/10.1103/PhysRevLett.81.5768
43. S.E. Hamann et al., Resolved-sideband Raman cooling to the ground state of an optical lattice. Phys. Rev. Lett. **80**(19), 4149–4152 (1998). doi:10.1103/PhysRevLett.80.4149. http://link.aps.org/doi/10.1103/PhysRevLett.80.4149

44. H. Perrin et al., Sideband cooling of neutral atoms in a far-detuned optical lattice. Europhys. Lett. (EPL) **42**(4), 395–400 (1998). ISSN: 0295-5075. doi:10.1209/epl/i1998-00261-y. http://iopscience.iop.org/0295-5075/42/4/395
45. A.M. Kaufman, B.J. Lester, C.A. Regal, Cooling a single atom in an optical tweezer to its quantum ground state. Phys. Rev. X**2**(4), 041014 (2012). doi:10.1103/PhysRevX.2.041014. http://link.aps.org/doi/10.1103/PhysRevX.2.041014
46. J.D. Thompson et al., Coherence and Raman sideband cooling of a single atom in an optical tweezer. Phys. Rev. Lett. **110**(13), 133001 (2013). doi:10.1103/PhysRevLett.110.133001. http://link.aps.org/doi/10.1103/PhysRevLett.110.133001
47. A.D. Boozer et al., Cooling to the ground state of axial motion for one atom strongly coupled to an optical cavity. Phys. Rev. Lett. **97**(8), 083602 (2006). doi:10.1103/PhysRevLett.97.083602. http://link.aps.org/doi/10.1103/PhysRevLett.97.083602
48. T. Puppe et al., Trapping and observing single atoms in a blue-detuned intracavity dipole trap. Phys. Rev. Lett. **99**(1), 013002 (2007). 00073, doi:10.1103/PhysRevLett.99.013002. http://link.aps.org/doi/10.1103/PhysRevLett.99.013002
49. E.D. Black, An introduction to Pound-Drever-Hall laser frequency stabilization. Am. J. Phys. **69**(1), 79 (2001). ISSN: 00029505. doi:10.1119/1.1286663. http://link.aip.org/link/AJPIAS/v69/i1/p79/s1&Agg=doi
50. S. Nußmann, Kühlen und Positionieren eines Atoms in einem optischen Resonator". 00000. PhD thesis. Technische Universität München (2006). http://mediatum.ub.tum.de/node?id=603119
51. C. Nölleke, Quantum state transfer between remote single atoms. 00000. PhD thesis. Technische Universität München (2013). http://mediatum.ub.tum.de/node?id=1145613
52. H. Specht, Einzelatom-Quantenspeicherfür Polarisations-Qubits. PhD thesis. Technische Universität München (2010). http://mediatum.ub.tum.de/node?id=1002627
53. A. Reiserer et al., Ground-state cooling of a single atom at the center of an optical cavity. Phys. Rev. Lett. **110**(22), 223003 (2013). doi:10.1103/PhysRevLett.110.223003. http://link.aps.org/doi/10.1103/PhysRevLett.110.223003
54. J. Bochmann et al., Lossless state detection of single neutral atoms. Phys. Rev. Lett. **104**(20), 203601 (2010). 00051, doi:10.1103/PhysRevLett.104.203601. http://link.aps.org/doi/10.1103/PhysRevLett.104.203601
55. Y. Colombe et al., Strong atom-field coupling for Bose-Einstein condensates in an optical cavity on a chip. Nature **450**(7167), 272–276 (2007). ISSN: 0028-0836.doi:10.1038/nature06331. http://www.nature.com/nature/journal/v450/n7167/abs/nature06331.html
56. A.J. Kerman et al., Beyond optical molasses: 3D Raman sideband cooling of atomic cesium to high phase-space density. Phys. Rev. Lett. **84**(3), 439–442 (2000). doi:10.1103/PhysRevLett.84.439. http://link.aps.org/doi/10.1103/PhysRevLett.84.439
57. D.J. Han et al., 3D Raman sideband cooling of cesium atoms at high density. Phys. Rev. Lett. **85**(4), 724–727 (2000). 00097, doi:10.1103/PhysRevLett.85.724. http://link.aps.org/doi/10.1103/PhysRevLett.85.724
58. A. Reiserer, S. Ritter, G. Rempe, Nondestructive detection of an optical photon. Science **342**(6164), 1349–1351 (2013). doi:10.1126/science.1246164. http://www.sciencemag.org/content/342/6164/1349
59. A. Reiserer et al., A quantum gate between a flying optical photon and a single trapped atom. Nature **508**(7495), 1349–1351 (2014). 00010, ISSN: 0028-0836. doi:10.1038/nature13177. http://www.nature.com/nature/journal/v508/n7495/full/nature13177.html

http://www.springer.com/978-3-319-26546-9

A Controlled Phase Gate Between a Single Atom and an Optical Photon

Reiserer, A.

2016, XIII, 72 p. 28 illus., Hardcover
ISBN: 978-3-319-26546-9